White Rose Research Online

eprints@whiterose.ac.uk
https://eprints.whiterose.ac.uk
Universities of Leeds, Sheffield and York

Deposited via The University of Sheffield.

White Rose Research Online URL for this paper:
https://eprints.whiterose.ac.uk/id/eprint/219513/

Version: Published Version

Article:
Nourafkan, E., Kenyon, C., Nair, A. et al. (2024) An experimental and modeling approach to study tangential flow filtration performance for mRNA drug substance purification. Biotechnology Journal, 19 (11). ISSN: 1860-6768

https://doi.org/10.1002/biot.202400473

Reuse
This article is distributed under the terms of the Creative Commons Attribution (CC BY) licence. This licence allows you to distribute, remix, tweak, and build upon the work, even commercially, as long as you credit the authors for the original work. More information and the full terms of the licence here: https://creativecommons.org/licenses/

Takedown
If you consider content in White Rose Research Online to be in breach of UK law, please notify us by emailing eprints@whiterose.ac.uk including the URL of the record and the reason for the withdrawal request.

UNIVERSITY OF LEEDS
University of Sheffield
UNIVERSITY of York

Biotechnology Journal

WILEY-VCH

Biotechnology Journal

RESEARCH ARTICLE OPEN ACCESS

An Experimental and Modeling Approach to Study Tangential Flow Filtration Performance for mRNA Drug Substance Purification

Ehsan Nourafkan[1] | Charlotte Kenyon[1] | Adithya Nair[1] | Kate A. Loveday[1] | Emma N. Welbourne[1] | Min Tao[1] | Mahdi Ahmed[1] | Joseph Middleton[1] | Mark J. Dickman[1] | Solomon F. Brown[1] | Mabrouka Maamra[1] | Joan Cordiner[1] | Zoltán Kis[1,2]

[1]Department of Chemical and Biological Engineering, University of Sheffield, Sheffield, UK | [2]Department of Chemical Engineering, Imperial College London, Roderic Hill Building, South Kensington Campus, SW7 2AZ, London, UK

Correspondence: Zoltán Kis (z.kis@sheffield.ac.uk)

Received: 31 July 2024 | **Revised:** 2 October 2024 | **Accepted:** 21 October 2024

Funding: This study was funded by the Wellcome Leap R3 program.

Keywords: Hermia model | membrane fouling | mRNA separation | tangential flow filtration | transmembrane pressure

ABSTRACT

Following the recent COVID-19 pandemic, mRNA manufacturing processes are being actively developed and optimized to produce the next generation of mRNA vaccines and therapeutics. Herein, the performance of the tangential flow filtration (TFF) was evaluated for high-recovery, and high-purity separation of mRNA from unreacted nucleoside triphosphates (NTPs) from the in vitro transcription (IVT) reaction mixture. For the first time, the fouling model was successfully validated with TFF experimental data to describe the adsorption of mRNA on filtration membrane. The fouling model enables monitoring of the mRNA purification processes, designing an appropriate strategy for filter clean-up, replacing the column at the right time and reducing the process cost. Recovery greater than 70% mRNA without degradation was obtained by implementing a capacity load of ~19 g/m^2, <2.5 psi transmembrane pressure (TMP) and feed flux of 300 LMH. This approach also enables the purification of multiple mRNA drug substance sequences for the treatment of a wide range of different diseases.

1 | Introduction

The transformative potential of the mRNA medicines platform technology is being recognized due to the COVID-19 pandemic, with a record-high number of RNA-based vaccines and therapeutics currently under development [1, 2]. This has led manufacturers to re-evaluate the associated procedures, guidelines, and production methodologies [3, 4]. Establishing a product- and indication-agnostic manufacturing process is highly advantageous [2, 5]. Due to the high-quality requirement and high cost of mRNA purification, it is desirable to remove impurities at the initial stages of the manufacturing process to avoid overloading the forthcoming unit operations [6]. During mRNA medicines manufacturing, mRNA drug substance concentration and buffer exchange might also be necessary to ensure the mRNA is ready for optimal purification through chromatography and/or encapsulation of mRNA in lipid nanoparticles (LNPs) [7]. This study deals with the separation of mRNA drug substance from unreacted materials directly after the in vitro transcription (IVT) reaction and preparing mRNA for the subsequent chromatography step.

Tangential flow filtration (TFF) or cross-flow filtration is a powerful membrane technology widely utilized in the biopharmaceutical industry for the size-based separation of macromolecules

This is an open access article under the terms of the Creative Commons Attribution License, which permits use, distribution and reproduction in any medium, provided the original work is properly cited.

© 2024 The Author(s). *Biotechnology Journal* published by Wiley-VCH GmbH.

from low molecular weight components. In TFF unit operations, the feed flows parallel or tangentially to the membrane plane, hence the name TFF. A part of this feed, containing molecules larger than the membrane pore size, is retained, and the other part of the feed, containing molecules smaller than the membrane pore size, permeates through the membrane surface. The feed and retentate sweep the filtration column surface, minimizing the filter fouling by reducing adsorption of (macro) molecules on the filter surface and inside the filter pores. This reduces membrane fouling and increases the permeate (aka. filtrate) flux compared to dead-end filtration; these are the advantages of TFF [8]. Concentration and diafiltration (DF) are two main operational modes of the TFF process. In concentration mode, the volume of the retentate is decreased while increasing the concentration of retained molecules. The DF mode involves the addition of fresh buffer such that the old buffer surrounding the (bio)macromolecule of interest (e.g., protein or mRNA) is exchanged for a buffer composition preferred for the next part of the vaccine manufacturing process.

TFF-based purification can also impact the stability of the mRNA. Funkner et al. compared RNA stability in both the IVT reaction mix and after mRNA separation with TFF [8]. The research revealed that higher stability was observed for purified mRNA as opposed to non-purified material. For instance, the high integrity of the TFF-separated mRNA was maintained for at least 7 days of room temperature storage, followed by a slow decrease in integrity to 80% by day 33. However, a rapid decrease in integrity to 51% was measured after 14 days for mRNA stored in the non-purified transcription reaction mixture. Funkner et al. also examined the separation of three different mRNA lengths (589, 1870, and 5337 nt) using 100, 300, and 1000 kDa spin filters [8]. The results showed that only 100 kDa molecular weight cut-off (MWCO) retained the three different lengths of mRNA completely.

In a recent study, Cui et al. carried out TFF process development using a KrosFlo KR2i TFF system to prepare the crude IVT reaction product for the chromatography step [9]. A 100 kDa MWCO mPES hollow fiber (HF) filters (Repligen) was used for the seperation of the impurites from IVT mixture. The effect of mRNA concentration on permeate flux was measured and used to find the best mRNA concentration range for performing the sepeartion process in this study. A weak decline of the permeate flow was reported for operation using an mRNA concentration below 1.5 mg/mL. Therefore, mRNA concentration <1.5 mg/mL, and preferably 1 mg/mL, was suggested for high permeate flux operation (>25 L/m^2/h [LMH]) for both short and long-chain mRNA molecules.

When developing a TFF process, the critical quality attributes (CQAs) of the mRNA product need to be maintained within acceptable ranges, as these CQA values translate to patient safety and product efficacy. The mRNA CQAs and associated acceptance criteria are determined based on pre-clinical and clinical data and can be identified from literature reviews, surveys of commercial manufacturers, United States Pharmacopeia guidelines and WHO technical reports [10–13]. The first objective of this study is to maintain the CQAs of mRNA in acceptable ranges by the end of the filtration process. For this purpose, the performance of TFF for separation, concentration and buffer exchange of mRNA drug substance (aka. "naked mRNA") was investigated by taking into account the mRNA CQAs (e.g., RNA integrity, residual nucleoside triphosphates [NTPs], and other product- and process-related impurities).

The authors believe there is a critical lack of understanding in the literature on mRNA loss due to membrane fouling. Therefore, as a second objective, we also aim to quantify the membrane fouling that occurs because of mRNA adsorption either on the surface of the filter and/or inside the filter pores. To achieve this, a detailed analysis was done to mathematically model the effect of mRNA membrane fouling on increasing filtration resistance and transmembrane pressure (TMP). Among models, the Hermia model which includes complete pore blocking, intermediate pore blocking, cake filtration, and standard pore blocking mechanisms, is a well-known framework for describing membrane fouling behavior. The model was used in several research studies to determine the fouling mechanism using mixtures of organic micro- and macro-molecules [14, 15]. In some of these studies, the Hermia model was applied to simulate the constant flux filtration processes [16, 17]. Here, we applied the Hermia model to cross-flow filtration to characterize the membrane fouling caused by mRNA and to investigate underlying mechanisms.

This paper is highly relevant as, addresses the significant gap in publicly available information on rigorous studies of mRNA processing, particularly focusing on TFF. The experimental and modeling results in this study are beneficial for developing and operating scalable TFF processes for mRNA manufacturing.

2 | Materials and Methods

In vitro transcription (IVT). mRNA was synthesized using IVT reactions that utilized template DNA at 2.66E-05 mM. The eGFP linearized template DNA was sourced from Aldevron and GenScript Biotech Corporation. DNA-dependent T7 RNA polymerase was acquired from Takara, Roche and New England Biolabs (NEB), and was used at final concentrations in the IVT such as 4.04×10^{-4} mM. Ribonucleotide triphosphates (ATP, CTP, GTP and UTP) were sourced from NEB and Roche. All NTPs were added to the IVT at equimolar ratios and at concentrations of up to 10 mM per ribonucleotide triphosphate. The IVT reaction was further supplemented with magnesium acetate, inorganic pyrophosphatase (Roche or NEB), RNase inhibitor (Roche or NEB), dithiothreitol (DTT), spermidine, and Triton-X-100 following IVT reaction compositions from the literature [18, 19]. The IVT reaction was incubated at 37°C for 2 h. For measuring RNA concentration by UV absorbance, the mRNA was purified from the IVT reaction mixture by Monarch RNA Cleanup Column (NEB) according to the manufacturer's recommended protocol. The mRNA from the TFF feed, retentate and permeate mRNA was quantified by anion exchange high-performance liquid chromatography (HPLC) [20].

TFF system and membrane pre-treatment. The mRNA filtration was conducted with a benchtop TFF system (KrosFlo KR2i, Repligen) and Spectrum mPES HF filter modules (Product number key: C02-E300-05-N 300 kDa, 20 cm^2) at room temperature (20.0°C ± 0.5°C). For each set of experiments, a new mPES HF filter was used. Any new filter modules were flushed using

18607314, 2024, 11, Downloaded from https://analyticalsciencejournals.onlinelibrary.wiley.com/doi/10.1002/biot.202400473 by Test, Wiley Online Library on [13/11/2024]. See the Terms and Conditions (https://onlinelibrary.wiley.com/terms-and-conditions) on Wiley Online Library for rules of use; OA articles are governed by the applicable Creative Commons License

deionized water according to manufacturer guidelines [21]. The accumulated mass of the retentate and permeate were measured with two digital balances at a 5-s interval. All the process parameters were recorded as a function of filtration time by a KF Comm 2 Software. The shear rate, which is particularly useful for scaling up the process, for different feed flow rates was calculated using the following equation [22]:

$$Shear\ rate = \frac{4Q}{n\pi r^3} \quad (1)$$

wherein Q is the flowrate (m^3/s), n is number of fibers in the hollow fiber module, and r is inner radius of the fiber (m).

Capillary gel electrophoresis. The integrity and size of mRNA were quantified by capillary gel electrophoresis (CGE) using an Agilent 5200 Fragment Analyser System with the Agilent RNA Kit (15 nt) according to the manufacturer's recommended protocol. mRNA was diluted to 50–100 ng/μL prior to analysis.

High-performance liquid chromatography (HPLC). The mRNA and NTPs concentrations were measured by anion exchange chromatography (AEX) at optimal conditions of: DNAPac PA200 as separation column, UV detection at a wavelength of 260 nm, sample injection volume was 5 μL, flow rate of 15 LMH and temperature of 25°C as explained in our previous work [20]. The errors of the CGE and IEX-HPLC methods are provided in Table S1.

3 | Results and Discussion

3.1 | Separation of mRNA From Unreacted NTPs Using TFF

Crude IVT consists of several components including mRNA product, unreacted NTPs, DNA template, T7 RNA polymerase, free ions and other impurities such as proteins. The filtration process is chosen to reduce impurity load before subsequent chromatography and/or to ensure suitable buffer for mRNA encapsulation. A typical TFF process usually involves three consecutive steps, this was applied for the separation of unreacted NTPs and recovery of deposited mRNA. At first, the volume of the diluted crude IVT inside the feed tank is decreased using concentration mode, hence a part of NTPs is separated at this step. Next, a DF step is carried out at flow rate equal to the permeate flux, where fresh buffer is injected into the system to wash out the remaining NTPs. Finally, a step is used to recover remaining mRNA inside the tubes and adsorbed ones on the membrane surface. In the first stage, a set of experiments including the three aforementioned steps was designed to evaluate the separation of the mRNA.

The eGFP crude IVT samples (5 mL, 7.5 ± 0.02 mg/mL) were diluted using Tris buffer pH 7 to 80 mL (0.468 mg/mL) to be used for the experiments. The experimental TFF tests were operated at constant permeate flux, and a hollow mPES fiber filter (300 kDa) was used for the separation of mRNA from unreacted NTPs. 5× concentration factor and 10× dilution factor were selected to fully separate unreacted NTPs (Figure 1). mRNA purity and integrity were monitored post-mPES membrane filtration.

Figure 1A,B illustrates the HPLC chromatograms of the collected samples after each step of the filtration process. The AEX HPLC results confirmed the complete separation of mRNA in the retentate: no mRNA peak was observed in the HPLC chromatogram of the collected permeate sample, showing that the selected membrane cut-off of 300 kDa retained all of the mRNA molecules. Moreover, no NTPs were detected in the retentate's chromatogram post DF, which confirms the complete separation of mRNA and NTPs by the end of the DF steps. A considerable amount of mRNA loss (between 30% and 40%) was observed post DF due to mRNA remaining inside both TFF tubes and filters as can be seen for concentration and DF parts in Figure 1C. Additionally, losses also occurred due to mPES membrane fouling. Washing the fouled membrane led to a significant recovery of the mRNA (>97%, post-washing steps in Figure 1C) which shows the importance of the filter washing. The mRNA integrity was assessed by CGE before and after the filtration. Figure 2 illustrates no change in shape and location of mRNA peak (~1000 nt) detection by CGE in electropherograms of TFF samples, confirming there was no mRNA degradation during the TFF process. The observed peak at 2000 nt that can be seen in crude IVT and retentate could be a multimer of eGFP transcripts or an unwanted by-product of the run-off transcription from a template that was not correctly linearized. The lower marker (LM) at 15 nt was added to ensure proper sizing of the sample during analysis. The LM is added during the loading process, and is not part of the sample.

The literature is limited about mRNA filtration; however, the available research articles stated that higher mRNA recovery is achieved when less mRNA is loaded onto the filter module (lower load capacity) and in combination with applying lower TMP. Cui et al. suggested loading capacities below 30 g/m^2 for mRNA TFF [9]. Scorza et al. reported applying the TFF technique for the separation of a 10 kb mRNA molecule from a crude IVT mixture using 500 kDa mPES filter (115 cm^2 membrane area). By applying low TMP (2 psi) and low shear rate (800 s^{-1}), the TFF method purified RNA with an overall recovery of 80% and is almost free from nucleotides [23].

In this study, overall recovery of 70% (concentration and DF part in Figure 1C) after the consecutive concentration and DF processes was obtained by implementing a capacity load of ~19 g/m^2, <2.5 psi TMP and feed flux of 300 LMH (shear rate of 1594 s^{-1}) without any mRNA degradation detected. The calculation for mRNA recovery and TMP profile during successive steps of concentration and DF are provided in the Supporting Information. However, overall an mRNA recovery of >97% was obtained after two post-washing steps (post-washing steps in Figure 1C). The TMP profile during successive stages of concentration and DF of mRNA is shown in Figure S1. Continuous TMP increase over time was observed during concentration mode because of the membrane fouling.

3.2 | Mathematical Modeling of Mass Balance in the TFF Operation

The general mass balance (MB) for solute i during TFF operation is given as [24]:

18607314, 2024, 11, Downloaded from https://analyticalsciencejournals.onlinelibrary.wiley.com/doi/10.1002/bmot.202400473 by Test, Wiley Online Library on [13/11/2024]. See the Terms and Conditions (https://onlinelibrary.wiley.com/terms-and-conditions) on Wiley Online Library for rules of use; OA articles are governed by the applicable Creative Commons License

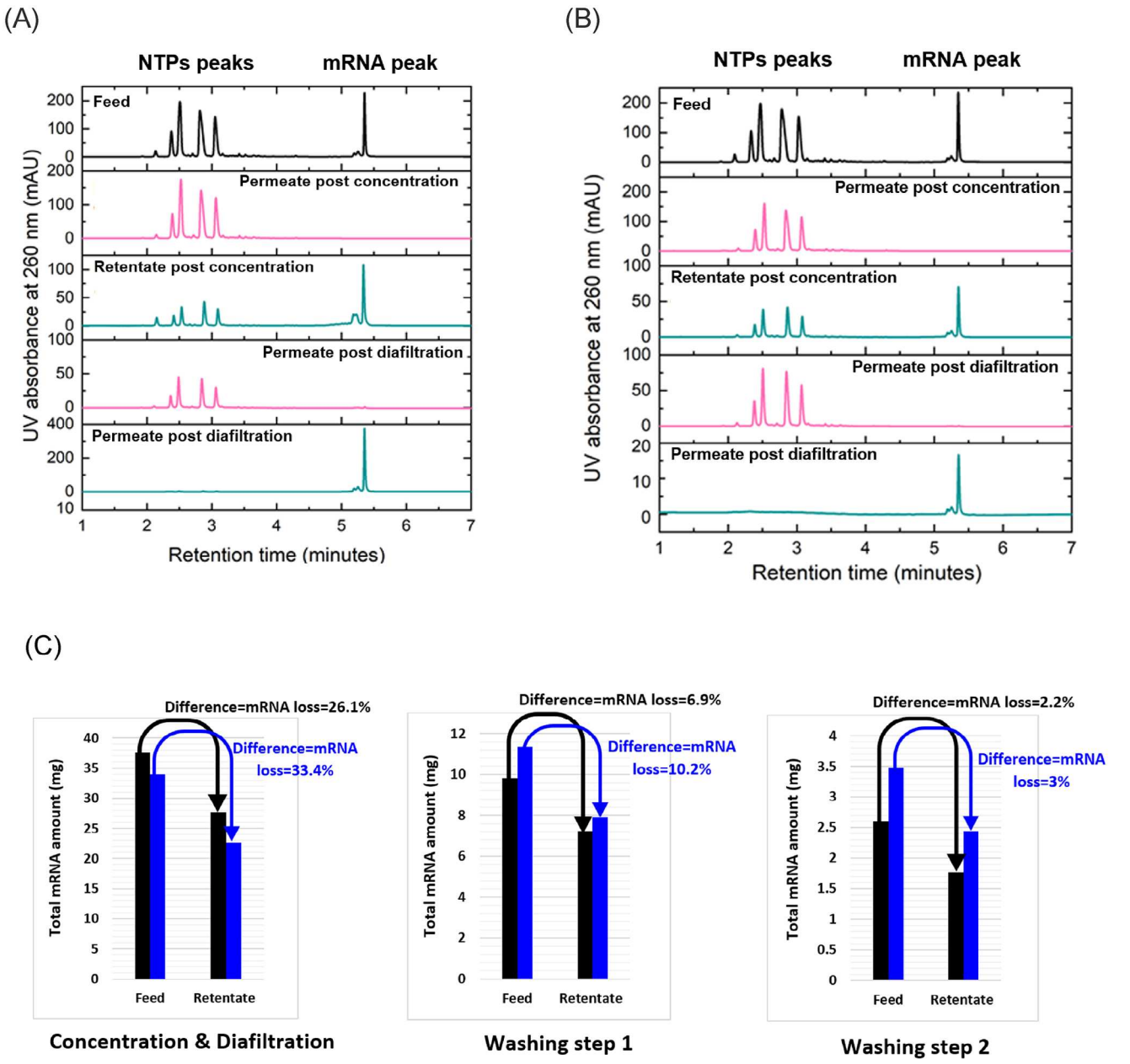

FIGURE 1 | Experimental TFF tests for mRNA separation from unreacted NTPs. (A) AEX HPLC chromatogram of test 1 and (B) test 1'; Test 1' (blue) is a replicate of Test 1 (black). (C) TFF concentration step followed by DF (con. factor: 5×, DF factor: 10×), washing step 1 (buffer volume: 20 mL) and washing step 2 (deionized water volume: 20 mL); The TFF experiment was run using 300 kDa MWCO mPES HF membrane filter at a constant permeate flux of 300 LMH (1594 s^{-1}). AEX, anion exchange chromatography; DF, diafiltration; HF, hollow fiber; HPLC, high-performance liquid chromatography; LMH, L/m^2/h; MWCO, molecular weight cut-off; NTPs, nucleoside triphosphates; TFF, tangential flow filtration.

$$\frac{d}{dt}\left(V_{\mathrm{FT}}(t)\,C_{\mathrm{FT},i}(t)\right) = C_{\mathrm{FT},i}(t)\,\frac{dV_{\mathrm{FT}}}{dt}(t) + V_{\mathrm{FT}}\,\frac{dC_{\mathrm{FT},i}}{dt}(t)$$
$$= DC_{D,i}(t) - P(t)\,C_{P,i}(t) \qquad (2)$$

where V_{FT} is feed tank volume (mL), $C_{TF,i}$, $C_{D,i}$, and $C_{P,i}$ are the concentration of solute i in the feed tank, DF buffer and permeate, respectively (mg/mL). D is DF buffer flow rate (mL/s), P is permeate flow rate (mL/s), i denotes solute i and t is time (s). In the DF tests, the feed tank volume was kept constant by controlling the DF flow rate ($\frac{dV_{\mathrm{FT}}}{dt} = 0$) using an auxiliary pump. The inlet flow equals the outlet flow ($P = D$). Therefore, Equation (2) is simplified to the below form [25]:

$$V_{FT}\frac{dC_{FT,i}(t)}{dt} = D\left(C_{D,i}(t) - C_{P,i}(t)\right)$$
$$\text{At time } t = 0 \qquad (3)$$
$$V_{FT}(0) = V_{FT}^{0}$$
$$C_{FT,i}(0) = C_{FT,i}^{0}$$

Equation (3) can be solved analytically or numerically [26, 27]. Here, the rejection factor was used to solve the Equation (3). The rejection factor, Equation (4), links the concentration of solute

18607314, 2024, 11, Downloaded from https://analyticalsciencejournals.onlinelibrary.wiley.com/doi/10.1002/biot.202400473 by Test, Wiley Online Library on [13/11/2024]. See the Terms and Conditions (https://onlinelibrary.wiley.com/terms-and-conditions) on Wiley Online Library for rules of use; OA articles are governed by the applicable Creative Commons License

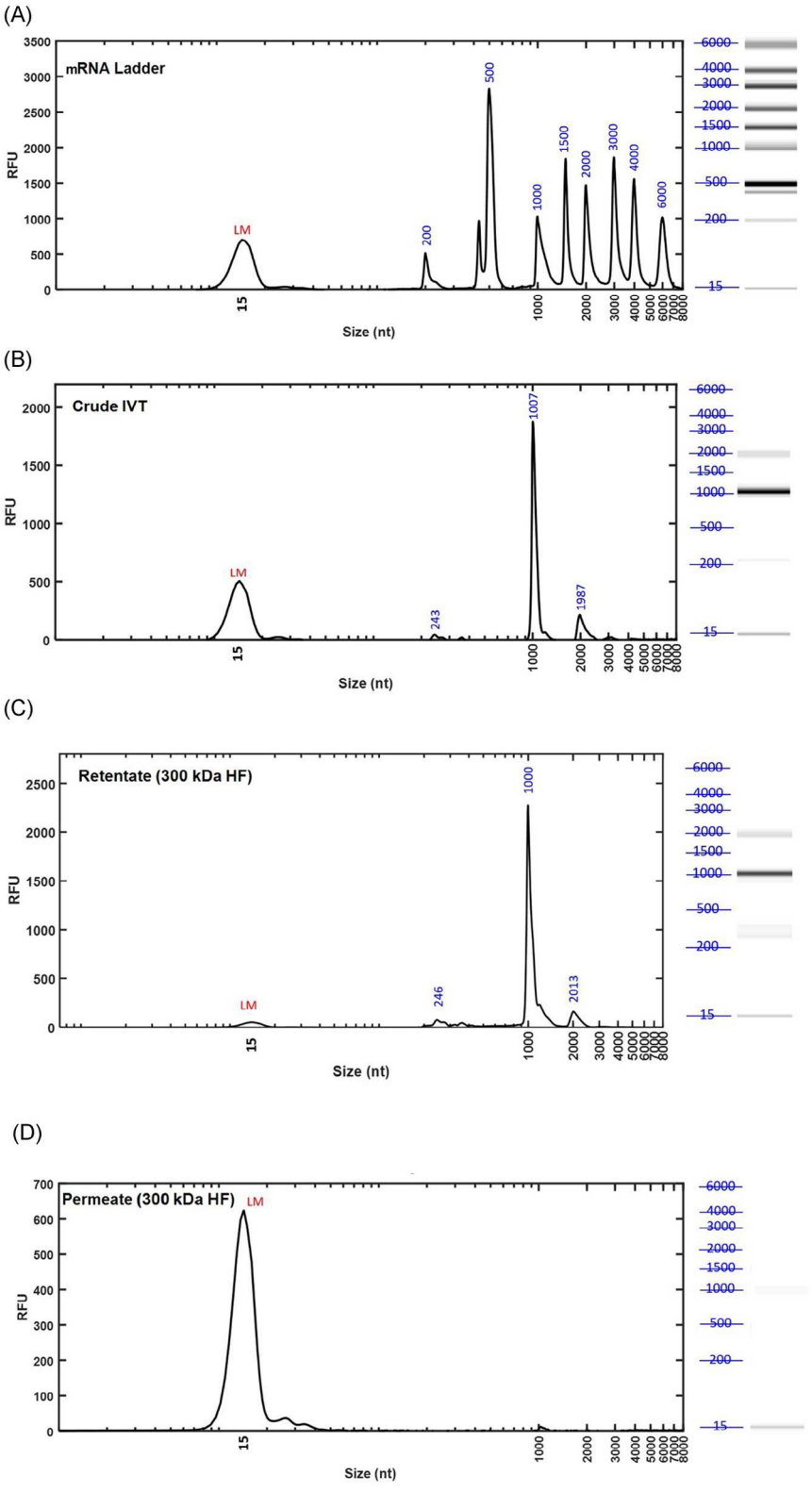

FIGURE 2 | Analysis of eGFP mRNA (1025 nt) separated using TFF. CGE results for (A) an RNA ladder, (A) a crude IVT, (C) collected retentate and (D) permeate at the end of the concentration run using the 300 kDa MWCO mPES HF membrane filter. *X*-axis in (C) and (D) shows the nucleotides size (nt) and *Y*-axis (RFU) shows the mRNA amount at a certain size/time. mRNA peak is around 1000 nt and the LM is at 15 nt. CGE, capillary gel electrophoresis; HF, hollow fiber; IVT, vitro transcription; LM, lower marker; RFU, relative fluorescence unit; TFF, tangential flow filtration.

18607314, 2024, 11, Downloaded from https://analyticalsciencejournals.onlinelibrary.wiley.com/doi/10.1002/bmot.202400473 by Test, Wiley Online Library on [13/11/2024]. See the Terms and Conditions (https://onlinelibrary.wiley.com/terms-and-conditions) on Wiley Online Library for rules of use; OA articles are governed by the applicable Creative Commons License

TABLE 1 | Experimental TFF DF tests for calculating the retention factor of eGFP mRNA (DF factor: 5×, mPES HF MWCO: 300 kDa and initial feed volume: 20 mL).

Test no.	2	3	4
Permeate flux (LMH)	30	70	90
NTP separation yield (%)	100	100	100
Overall mRNA loss (%)	36	27	18
Total time of process (min)	112	45	38

Abbreviations: DF, diafiltration; LMH, L/m^2/h; NTP, nucleoside triphosphate.

between feed and permeate flows and refers to the ability of the membrane to prevent the passage of mRNA, while allowing the low MW molecules (e.g., NTPs) to pass through it [24, 27].

$$R_i(t) = 1 - \frac{C_{P,i}(t)}{C_{\mathrm{FT},i}(t)} \tag{4}$$

The rejection factor can be affected by several parameters and variables, including the size of solute, membrane characteristics (e.g., pore size and surface chemistry), and buffer properties (e.g., viscosity or ionic strength) [28]. By assuming that the microsolutes and macrosolutes are not affected by the dynamics of the concentration step in the feed tank, the rejection factor can be considered a constant value. With this assumption, and by taking into consideration that there are no mRNA and NTP molecules in the DF buffer ($C_{D,i} = 0$), the analytical solution for Equation (3) is as follows [24]:

$$\begin{aligned} &R_i(t) = \partial = \text{constant} \\ &C_{FT,i}(t) = C_{FT,i}(0)\, e^{\frac{D(\partial-1).t}{V_{FT}}}, \text{ at the end of test}: \; D.t_f = V_b \\ &C_{FT,i}\left(t_f\right) = C_{FT,i}(0)\, e^{\frac{V_b(\partial-1)}{V_{FT}}} \end{aligned} \tag{5}$$

A set of experimental tests (cf. Table 1) were carried out in DF mode (5× dilution factor) at constant permeate flux in order to fit Equation (5) with the experimental observation and examine the accuracy of the analytical solution for this case study. The eGFP crude IVT samples (1 mL, 7.6 ± 0.02 mg/mL) were diluted using Tris buffer (10 mM, pH 7) to 20 mL (0.38 mg/mL) to be used for the experiments. A new Hollow mPES fiber filter (300 kDa) was used for each experiment. Several samples were taken at specific time intervals through a microfluidic valve connected to the retentate flow and analyzed by AEX HPLC to quantify the NTP depletion over time.

The TMP profile of the tests is included in Figure S2. The tiny jumps of the pressure in the TMP profile are due to the sampling process through the retentate line for analytics. The observed TMP decrease over time can be attributed to a reduction of the buffer viscosity in the storage tank with the depletion of NTPs. Higher permeate fluxes lead to a sharper decrease in TMP over time due to the faster NTP depletion. The analytical solution, Equation (5), was fitted to NTP concentration data by minimizing the Mean Squared Error (MSE), Equation (6).

$$\mathrm{MSE} = \frac{1}{N}\sum_{i=1}^{N}\left(y_{exp}(i) - y_{mod}(i)\right)^2 \tag{6}$$

where y_{exp} and y_{mod} are experimental observation and model estimation, respectively; N is the number of experiments. The coefficient of determination ($R^2 = 0.96$) shows the model accuracy in estimating NTP depletion during the DF process (Figure 3A). The variation of the NTP's rejection factor as a function of feed flux is shown in Figure 3B, which is in agreement with the range of rejection factors reported in the literature for other case studies [27, 29]. The rejection factor for eGFP mRNA (1023 nt) is equal to 1 for the 300 kDa MWCO mPES HF filter module since no mRNA was observed in the permeate. Most mRNA molecules of vaccine or therapeutics relevance would have a size larger than eGFP reporter gene, therefore the rejection factor would remain 1. The rejection factor could be less than 1 for smaller mRNA molecules which may pass through filter membrane pores. However, this is much less relevant for vaccine or therapeutic applications. In such cases, filter membranes with lower cut-off than 300 kDa (e.g., 100 kDa MWCO) could be used to separate, concentrate and buffer-exchange mRNA.

3.3 | Membrane Fouling in TFF Process for mRNA Purification

Membrane fouling is the primary problem limiting the application of membrane filtration [30, 31]. It is crucial to develop an effective model that accurately predicts the TMP that guides us to optimize the membrane cleaning to recover fouled mRNA. The volumetric flow rate through the TFF filter can be described by the resistance-in-series model based on Darcy's Law shown below [32, 33]:

$$\begin{aligned} Q &= \frac{\mathrm{TMP}.a}{\mu\left(R_m + R_g\right)} \\ R_m &= R_I + R_p \end{aligned} \tag{7}$$

where Q is volumetric flow rate (m^3/s), a is unobstructed (clean, unfouled) membrane surface area (m^2), μ is viscosity (N.s/m^2), R_g, R_m, R_I, and R_p are gel layer resistance (m^{-1}), membrane resistance, intrinsic membrane resistance, and membrane pore resistance, respectively (m^{-1}). The total resistance is described by the summation of resistance, including the membrane itself and the resistances due to gel layer formation. The nature of membrane fouling can be reversible or irreversible [34]. According to the experimental observation in Section 4, almost full recovery (loss of around 3%) of deposited mRNA was achieved post-washing of the membrane. This means that the irreversible resistance is almost zero for mRNA constructs used in this study. The intrinsic resistance of the virgin membrane was calculated to be $R_I = 2.44 \times 10^{14}$ m^{-1} for 300 kDa HF membranes by fitting the permeate flux versus TMP pressure for a clean membrane (Figure S3 for details about the intrinsic resistance calculation). Intrinsic membrane resistance is a useful parameter for designing an appropriate methodology for both membrane cleaning and membrane life-span determination.

The schematic of mechanisms of the Hermia model for mRNA fouling is illustrated in Figure 4. In the early stage of the filtration process, the mRNA molecules adhere to the mPES membrane surface and block some of the pores. Over time, the mRNA molecules link together, and a gel layer starts to form on the

18607314, 2024, 11, Downloaded from https://analyticalsciencejournals.onlinelibrary.wiley.com/doi/10.1002/biot.202400473 by Test, Wiley Online Library on [13/11/2024]. See the Terms and Conditions (https://onlinelibrary.wiley.com/terms-and-conditions) on Wiley Online Library for rules of use; OA articles are governed by the applicable Creative Commons License

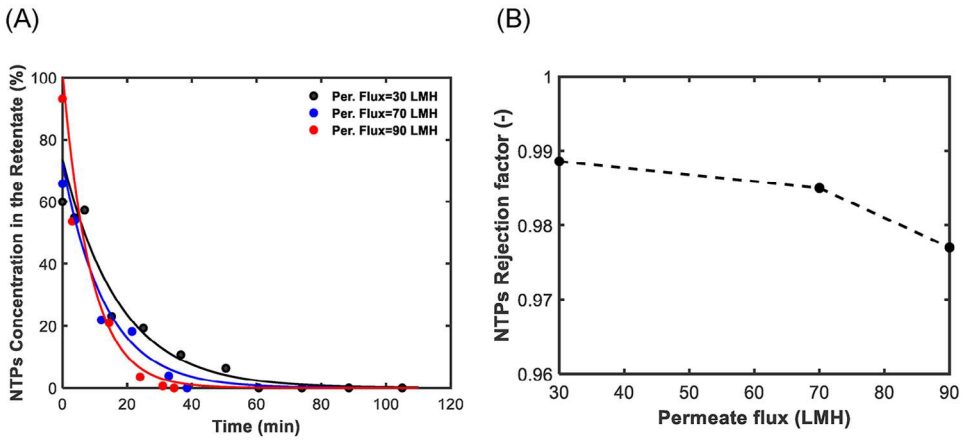

FIGURE 3 | Separation of NTPs from mRNA over time at different permeate fluxes. (A) Circle points correspond to experimental data (AEX HPLC measurements of NTPs), and the line corresponds to the model predictions. (B) The variation of rejection factor calculated from the mass balance after fitting the model with the experimental data at various permeate fluxes. Results were obtained using the 300 kDa mPES HF membrane. AEX, anion exchange chromatography; HF, hollow fiber; HPLC, high-performance liquid chromatography; NTPs, nucleoside triphosphates.

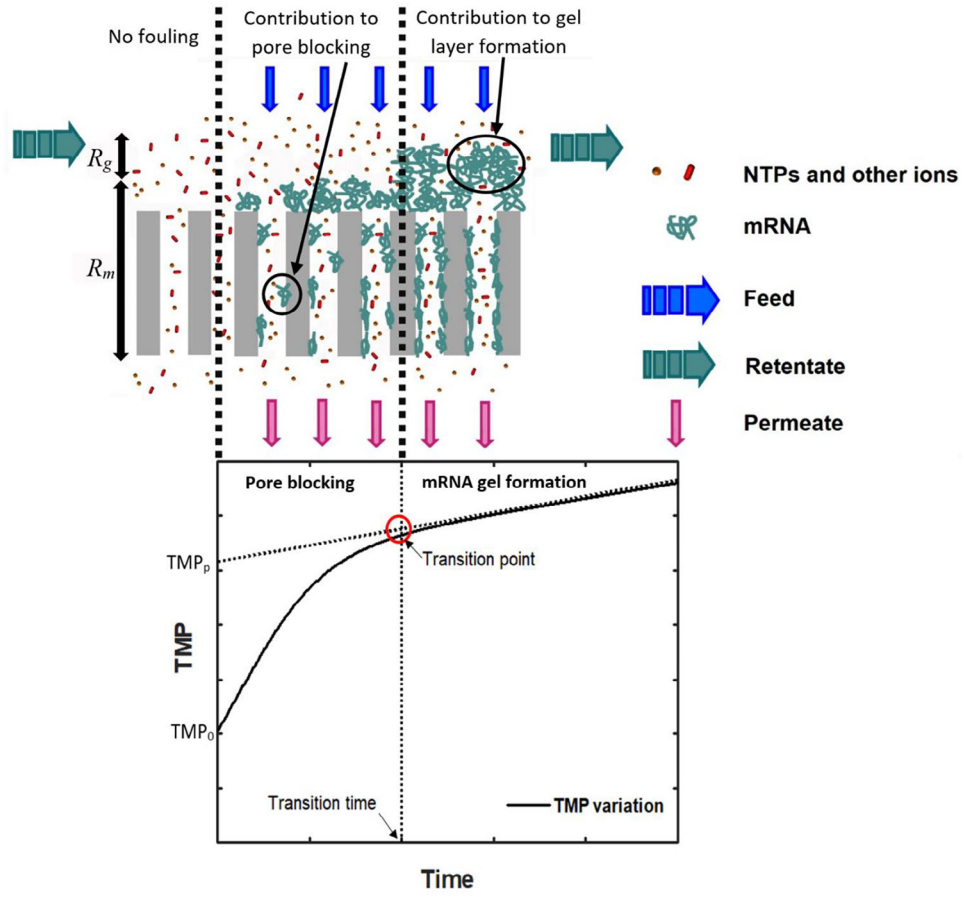

FIGURE 4 | TFF membrane fouling based on the Hermia model. Schematic representation of Hermia's fouling mechanisms caused by mRNA, and the variation of TMP over time based on the proposed model. TFF, tangential flow filtration; TMP, transmembrane pressure.

membrane surface; however, some pores may still remain open. The standard blocking model states that mRNA can penetrate into the pores and adhere to the pore walls. In fact, the TMP profile includes two separate regions, the partial pressure of the membrane layer (TMP_m), and the partial pressure of the gel layer (TMP_g) [17]. Equation (7) can be rewritten for the different stages of the constant flux filtration process as follows:

$$\frac{TMP_m}{R_m} = \frac{TMP_g}{(R_m + R_g)} = \mu J \tag{8}$$

where J is permeate flux (m/s).

18607314, 2024, 11, Downloaded from https://analyticalsciencejournals.onlinelibrary.wiley.com/doi/10.1002/bbot.202400473 by Test, Wiley Online Library on [13/11/2024]. See the Terms and Conditions (https://onlinelibrary.wiley.com/terms-and-conditions) on Wiley Online Library for rules of use; OA articles are governed by the applicable Creative Commons License

TABLE 2 | Experimental TFF concentration tests for membrane fouling analysis of eGFP mRNA and the optimum value of proposed model's parameters (5× con. factor, mPES HF MWCO: 300 kDa and initial feed volume: 20 mL).

Test no.	5	6	7	8
Permeate flux (LMH)	30	40	70	90
mRNA loss (%)	29.5	42.8	52.4	51.8
Total time of process (min)	26	14	10	7
B **(s^{-1})**	0.72	0.84	0.98	1.04
Ki	2.55	5.28	7.7	9.1
Kc **($\times 10^6$ m^{-1})**	0	0	1.21	1.62

The transition point has been determined by a red circle in Figure 4 and at this point, changing from pore-blocking mechanism to cake filtration (i.e., gel layer formation) is happened. Therefore, and as shown by the Equation (9), the overall TMP is the summation of the partial pressure of these two regions.

$$\mathrm{TMP} = \mathrm{TMP}_m + \mathrm{TMP}_g \tag{9}$$

Here, the combined model of intermediate pore blocking and cake filtration mechanisms developed by Krischner, Equation (10), was employed to model the mRNA fouling on an mPES HF membrane [35].

$$\mathrm{TMP} = \mathrm{TMP}_0 \times \left[\frac{1}{\frac{1}{K_i} + \left(1 - \frac{1}{K_i}\right) \exp\left(-K_i B t\right)} + (1 + K_C J t) \right] \tag{10}$$

where K_c is cake filtration constant for crossflow filtration (m^{-1}), K_i is intermediate pore blocking constant (-) and B is particle resuspension rate (s^{-1}).

Constant permeate flux experiments were conducted (Table 2) and TMP was recorded over time (Figure 5). The eGFP crude IVT samples (1 mL, 7.6 ± 0.02 mg/mL) were diluted using Tris buffer (10 mM, pH 7) to 20 mL (0.38 mg/mL) to be used for the experiments. A new Hollow mPES fiber filter (300 kDa) was used to perform a test operated at a 5× concentration factor. In the intermediate pore-blocking mechanism, TMP initially sharply increases and then approaches a plateau, which can explain the TMP trend at low flux. The plateau in TMP indicates an equilibrium between mRNA molecules adsorbed onto the membrane surface and mRNA molecules removed from the surface by crossflow shear. At higher fluxes, the initial sharp rise is followed by a continued slower rise, rather than a plateau in pressure. This behavior is associated with mRNA gel layer formation when the mRNA concentration is high in the feed storage tank. In fact, both high mRNA concentration in the feed tank and high crossflow shear will induce the mass transfer rate into the gel layer on filter surface [36]. At the start of filtration test, adsorption of mRNA molecules on open pores is the main fouling mechanism (i.e., intermediate pore- blocking mechanism), while and once enough mRNA accumulation saturated the membrane surface, the gel layer formation is the dominant mechanism for TMP controlling.

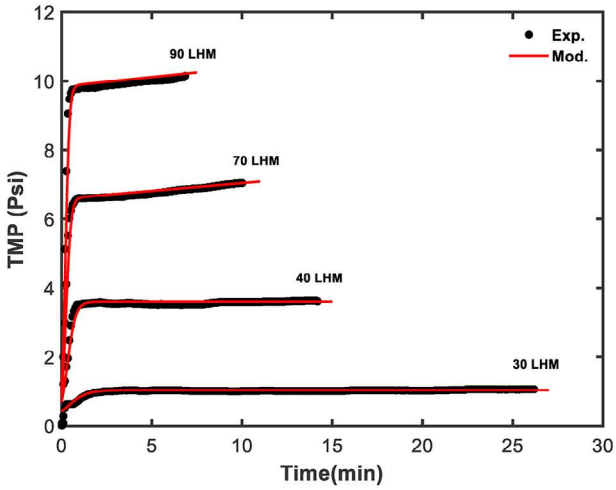

FIGURE 5 | Comparison of experimental data with model fits for filtration of eGFP mRNA. The experimental tests were done at constant permeate flux and the combined intermediate pore blocking and cake filtration model, Equation (10), was used for data fitting.

The Hermia model fitting with experimental data suggests a transition between two mechanisms of fouling at high flow rates: intermediate pore blocking and gel layer formation (Figure 5). The model parameters (B, K_i, K_c) were obtained by a fitting method (minimizing the MSE) (Table 2). K_i and K_c raised with the increase of the flux, due to an increase in deposition of mRNA on the membrane surface at the higher permeate flux. A higher value of the B parameter indicates a greater probability of the mRNA molecule being removed from the membrane surfaces. The probability is larger at higher permeate flux when a higher number of mRNA molecules have been deposited [37]. The increasing trend of K_i, K_c, and B parameters as a function of permeate flux is illustrated in Figure S4. At higher fluxes, the increase of membrane fouling due to higher crossflow shear (i.e., accelerating mRNA adsorption) exceeds its positive effect of removing mRNA. This is why the rate of increase of K_i and K_c parameters is steeper than that of the B parameter (cf. Figure S4).

Xing et al. simulated these experimental findings using computational fluid dynamics (CFD) to assess the effect of shear stress on foulant deposition. The CFD model result confirmed that lower shear stress could reduce membrane fouling, while the higher shear stress enhances membrane fouling [38] aligning with our observation. However, other studies have challenged

18607314, 2024, 11, Downloaded from https://analyticalsciencejournals.onlinelibrary.wiley.com/doi/10.1002/biot.202400473 by Test, Wiley Online Library on [13/11/2024]. See the Terms and Conditions (https://onlinelibrary.wiley.com/terms-and-conditions) on Wiley Online Library for rules of use; OA articles are governed by the applicable Creative Commons License

this, disputing the reduction of membrane fouling by shear stress at higher permeate fluxes [39].

TFF membrane fouling caused by mRNA can be reduced by: (1) operating at a lower permeate flux, (2) operating at a lower TMP, (3) increasing crossflow velocity to enhance the sweeping action across the membrane surface, (4) using a membrane with a pore size (MWCO) which is not too low (e.g., at least 100 or 300 kDa); (5) lowering the mRNA concentration in the feed and in the retentate; (6) washing/cleaning the filter membrane.

The TFF process enables the separation, purification, concentration, and buffer exchange of both the mRNA drug substance and the drug product. However, membrane fouling remains a significant concern for both drug substance and drug product TFF processes [9, 40]. Common examples of mRNA drug products include various lipid-based formulations, for example, LNPs [41]. These mRNA drug product TFF processes often come with their own challenges related to obtaining the desired product quality attributes under efficient manufacturing conditions (e.g., minimal product losses).

4 | Conclusion

The results from this study are directly applicable to the development of membrane systems for the preparation of mRNA-based vaccines and therapeutics. In this study, full separation of mRNA drug substance from unreacted NTPs with high recovery and preservation of mRNA integrity was achieved through a series of TFF experimental tests. TFF-based drug product purification, such as the removal of organic solvents (e.g., ethanol) through buffer exchange, along with the associated membrane fouling, is currently under investigation. The results will be published in a separate paper. The impact of permeate flux on mRNA recovery was investigated for both concentration and DF mode. Firstly, for concentration mode, lower permeate fluxes (<40 LMH and <1 mg/mL) are preferred for achieving a stable TMP profile. Over 97% of the of mRNA can be recovered by washing the membrane via a two-stage recovery step at the end of the concentration process. Secondly, for DF, higher permeate fluxes can speed up the TFF process. During DF, the most significant factor impacting membrane fouling is mRNA concentration and this factor remains constant in the feed tank. Both the depletion of NTPs from the feed stream and the addition of fresh buffer to the feed stream prevent TMP from rising during DF. Moreover, a MB approach was used to model the DF process, and a Hermia-based model was fitted to TMP over a wide range of filtrate fluxes in concentration mode. These models enhance the understanding of mRNA processing by TFF, guide TFF process development, can define a design space and improve TFF operation. The strong fit of the experimental data to the MB model suggests that the NTPs rejection factor is independent of concentration levels in the feed tank. This allows the total DF time to be estimated across a range of permeate fluxes. TFF filter fouling and the resulting increase in transport resistance were particularly significant during the concentration of the mRNA drug substance. The Hermia model effectively predicts the TMP over time, and any deviation from the predicted values could indicate an issue in the filtration process (e.g., fouling caused by magnesium pyrophosphate precipitation in the diluted crude IVT). The fouling analysis also provided an estimate for when the TFF filter should be replaced, based on a considerable difference between the membrane's intrinsic resistance and resistance observed after membrane washing.

Nomenclature

K_c	Cake filtration constant for crossflow filtration, m^{-1}
K_i	intermediate pore blocking constant, (-)
K_s	standard pore blocking constant, m^{-3}
R_I	intrinsic membrane resistance, m^{-1}
R_g	gel layer resistance, m^{-1}
R_m	membrane resistance, m^{-1}
R_p	membrane pore resistance, m^{-1}
TMP_c	transmembrane pressure originating from cake resistance, N/m^2
TMP_p	transmembrane pressure originating from pore blocking/shrinking resistance, N/m^2
V_{FT}	feed tank volume, mL
V_b	total volume of diafiltration buffer, mL
t_f	time final, s
LMH	unit of measurement for flux, $L/m^2/h$
r	inner radius of the fiber (m)
RFU	relative fluorescence units (-)
B	particle resuspension rate, s^{-1}
C	concentration, mg/mL
D	diafiltration buffer flow rate, mL/s
FT	feed tank outflow flow rate, mL/s
J	permeate flux, m/s
P	permeate flow rate, mL/s
Q	volumetric flow rate, m^3/s
R	rejection factor, (-)
	transmembrane pressure, N/m^2
a	unobstructed (clean, unfouled) membrane surface area, m^2
i	denote solute i, (-)
n	number of fibers in the hollow fiber module, (-)
nt	number of nucleotides in mRNA molecule, (-)
t	time, s
μ	viscosity, $N.s/m^2$
σ	blocked area per unit filtrate volume, m^{-1}
∂	constant rejection factor, (-)

Author Contributions

Ehsan Nourafkan designed, and performed the tests, modeled the process, and wrote the original draft. Charlotte Kenyon, Adithya Nair, and Kate A. Loveday performed a part of the experimental tests and analysis. Emma N. Welbourne did HPLC analysis under Mark J. Dickman supervision. Mabrouka Maamra worked as project manager. Solomon F. Brown, Joan Cordiner, and Zoltán Kis responsible for supervision and funding acquisition. The authors have reviewed and edited the manuscript.

18607314, 2024, 11, Downloaded from https://analyticalsciencejournals.onlinelibrary.wiley.com/doi/10.1002/bmot.202400473 by Test, Wiley Online Library on [13/11/2024]. See the Terms and Conditions (https://onlinelibrary.wiley.com/terms-and-conditions) on Wiley Online Library for rules of use; OA articles are governed by the applicable Creative Commons License

Acknowledgments

This study was funded by the Wellcome Leap R3 Program. The funder played no role in study design, data collection, analysis and interpretation of data, or the writing of this manuscript. The work was supported by the School of Chemical, Materials and Biological Engineering (formerly Department of Chemical and Biological Engineering), University of Sheffield, UK.

Conflicts of Interest

The authors declare that there is not any known competing financial interests or personal relationships that could have appeared to influence the work reported in this paper.

Data Availability Statement

The data that support the findings of this study are available from the corresponding author upon reasonable request.

References

1. S. Qin, X. Tang, Y. Chen, et al., "mRNA-Based Therapeutics: Powerful and Versatile Tools to Combat Diseases," *Signal Transduction and Targeted Therapy* 7 (2022): 166.

2. World Health Organization. *Potential Benefits and Limitations of mRNA Technology for Vaccine Research and Development for Infectious Diseases and Virus-Induced Cancers: Report of the WHO Science Council* (World Health Organization, 2023).

3. J. Whitley, C. Zwolinski, C. Denis, et al., "Development of mRNA Manufacturing for Vaccines and Therapeutics: mRNA Platform Requirements and Development of a Scalable Production Process to Support Early Phase Clinical Trials," *Translational Research* 242 (2022): 38–55.

4. W. Mao, A. Zimmerman, E. U. Hodges, et al., "Comparing Research and Development, Launch, and Scale up Timelines of 18 Vaccines: Lessons Learnt From COVID-19 and Implications for Other Infectious Diseases," *BMJ Global Health* 8 (2023): e012855.

5. N. Jackson, K. Kester, D. Casimiro, S. Gurunathan, and F. DeRosa, "The Promise of mRNA Vaccines: A Biotech and Industrial Perspective," *NPJ Vaccines* 5 (2020): 11.

6. G. T. Szabó, A. J. Mahiny, and I. Vlatkovic, "COVID-19 mRNA Vaccines: Platforms and Current Developments," *Molecular Therapy* 30 (2022): 1850–1868.

7. K. Nag, M. E. H. Sarker, S. Kumar, et al., "DoE-Derived Continuous and Robust Process for Manufacturing of Pharmaceutical-Grade Wide-Range LNPs for RNA-Vaccine/Drug Delivery," *Scientific Reports* 12 (2022): 9394.

8. A. Funkner, S. Dorner, S. Sewing, et al. Method for Producing and Purifying RNA, Comprising at Least one Step of Tangential Flow Filtration. World Intellectual Property Organization, WO2016193206A1 (2020).

9. T. Cui, K. Fakhfakh, H. Turney, et al., "Comprehensive Studies on Building a Scalable Downstream Process for mRNAs to Enable mRNA Therapeutics," *Biotechnology Progress* 39 (2023): e3301.

10. S. Daniel, Z. Kis, C. Kontoravdi, and N. Shah, "Quality by Design for Enabling RNA Platform Production Processes," *Trends in Biotechnology* 40 (2022): 1213–1228.

11. World Health Organization. *Evaluation of the Quality, Safety and Efficacy of Messenger RNA Vaccines for the Prevention of Infectious Diseases: Regulatory Considerations* (World Health Organization, 2022).

12. *Analytical Procedures for Quality of mRNA Vaccines and Therapeutics* (United States Pharmacopeia, 2023).

13. World Health Organization. *WHO Expert Committee on Biological Standardization: Seventy-Fourth Report* (World Health Organization, 2022).

14. K. Gao, T. Li, J. Liu, B. Dong, and H. Chu, "Ultrafiltration Membrane Fouling Performance by Mixtures With Micromolecular and Macromolecular Organics," *Environmental Science: Water Research & Technology* 5 (2019): 277–286.

15. B. Niu, L. Yang, S. Meng, et al., "Time-Dependent Analysis of Polysaccharide Fouling by Hermia Models: Reveal the Structure of Fouling Layer," *Separation and Purification Technology* 302 (2022): 122093.

16. M. Kim, B. Sankararao, S. Lee, and C. Yoo, "Prediction and Identification of Membrane Fouling Mechanism in a Membrane Bioreactor Using a Combined Mechanistic Model," *Industrial & Engineering Chemistry Research* 52 (2013): 17198–17205.

17. X. Du, Z. Wang, and L. Chao, "A Combined Model for Describing the Trans-Membrane Pressure (P) Variation in Constant Flux Dead-end Microfiltration (MF) Process," *Journal of Environmental Chemical Engineering* 10 (2022): 107076.

18. D. van De Berg, Z. Kis, C. F. Behmer, et al., "Quality by Design Modelling to Support Rapid RNA Vaccine Production Against Emerging Infectious Diseases," *Npj Vaccines* 6 (2021): 65.

19. K. Samnuan, A. K. Blakney, P. F. McKay, and R. J. Shattock, "Design-of-Experiments in Vitro Transcription Yield Optimization of Self-Amplifying RNA," *BioRxiv* (2021): 2021–2001.

20. E. N. Welbourne, K. A. Loveday, A. Nair, et al., "Anion Exchange HPLC Monitoring of mRNA in Vitro Transcription Reactions to Support mRNA Manufacturing Process Development," *Frontiers in Molecular Biosciences* 11 (2024): 1250833.

21. Hollow Fiber Filter Module Preparation & Instruction Guide, 400-12058-000 Rev. 05–150107. Repligen 2024, https://www.repligen.com/Products/Hollow%20Fibers/Spectrum_Hollow_Fiber_Filters/Hollow_Fiber_Filter_Module_Preparation_UserGuide_30Jun2015.pdf.

22. A. Mitterer, M. Hasslacher, and C. Mayer. Method of Concentrating Shear-Sensitive Biopolymers Using Hollow Fibre Membranes. CN102137708A (2009).

23. F. B. Scorza, Y. Wen, A. Geall, and F. Porter. RNA purification methods. US20210214388A1 (2021).

24. Z. Kovacs, M. Fikar, and P. Czermak, "Mathematical Modeling of Diafiltration," *Hungarian Journal of Industrial Chemistry* 37 (2009): 159–164.

25. R. Ambrožič, D. Arzenšek, and A. Podgornik, "Designing Scalable Ultrafiltration/Diafiltration Process of Monoclonal Antibodies via Mathematical Modeling by Coupling Mass Balances and Poisson–Boltzmann Equation," *Biotechnology and Bioengineering* 118 (2021): 633–646.

26. Z. Kovács, M. Discacciati, and W. Samhaber, "Modeling of Batch and Semi-Batch Membrane Filtration Processes," *Journal of Membrane Science* 327 (2009): 164–173.

27. L. Wang, T. Cao, J. E. Dykstra, S. Porada, P. M. Biesheuvel, and M. Elimelech, "Salt and Water Transport in Reverse Osmosis Membranes: Beyond the Solution-Diffusion Model," *Environmental Science & Technology* 55 (2021): 16665–16675.

28. H. Q. Dang, L. D. Nghiem, and W. E. Price, "Factors Governing the Rejection of Trace Organic Contaminants by Nanofiltration and Reverse Osmosis Membranes," *Desalination and Water Treatment* 52 (2014): 589–599.

29. X. Ma, P. Chen, M. Zhou, Z. Zhong, F. Zhang, and W. Xing, "Tight Ultrafiltration Ceramic Membrane for Separation of Dyes and Mixed Salts (both $NaCl/Na_2SO_4$) in Textile Wastewater Treatment," *Industrial & Engineering Chemistry Research* 56 (2017): 7070–7079.

30. Z. Wang, J. Ma, C. Y. Tang, K. Kimura, Q. Wang, and X. Han, "Membrane Cleaning in Membrane Bioreactors: A Review," *Journal of Membrane Science* 468 (2014): 276–307.

31. F. Meng, S. Zhang, Y. Oh, Z. Zhou, H.-S. Shin, and S.-R. Chae, "Fouling in Membrane Bioreactors: An Updated Review," *Water Research* 114 (2017): 151–180.

18607314, 2024, 11, Downloaded from https://analyticalsciencejournals.onlinelibrary.wiley.com/doi/10.1002/biot.202400473 by Test, Wiley Online Library on [13/11/2024]. See the Terms and Conditions (https://onlinelibrary.wiley.com/terms-and-conditions) on Wiley Online Library for rules of use; OA articles are governed by the applicable Creative Commons License

32. Y. Shimizu, K.-I. Shimodera, and A. Watanabe, "Cross-Flow Microfiltration of Bacterial Cells," *Journal of Fermentation and Bioengineering* 76 (1993): 493–500.

33. P. K. Watler and J. Rozembersky, "Application of QbD Principles to Tangential Flow Filtration operations," *Quality by Design for Biopharmaceuticals: Principles and Case Studies*. (Hoboken: Wiley, 2009), 111–126.

34. C. Quezada, H. Estay, A. Cassano, E. Troncoso, and R. Ruby-Figueroa, "Prediction of Permeate Flux in Ultrafiltration Processes: A Review of Modeling Approaches," *Membranes* 11 (2021): 368.

35. A. Y. Kirschner, Y.-H. Cheng, D. R. Paul, R. W. Field, and B. D. Freeman, "Fouling Mechanisms in Constant Flux Crossflow Ultrafiltration," *Journal of Membrane Science* 574 (2019): 65–75.

36. Z. Wang, J. Chu, and X. Zhang, "Study of a Cake Model During Stirred Dead-End Microfiltration," *Desalination* 217 (2007): 127–138.

37. Z. He, D. J. Miller, S. Kasemset, D. R. Paul, and B. D. Freeman, "The Effect of Permeate Flux on Membrane Fouling During Microfiltration of Oily Water," *Journal of Membrane Science* 525 (2017): 25–34.

38. D. Xing, K. Zhang, H. Yang, et al., "The Relationship Between Size-Segregated Particles Migration Phenomenon and Combined Membrane Fouling in Ultrafiltration Processes: The Significance of Shear Stress," *Journal of the Taiwan Institute of Chemical Engineers* 96 (2019): 45–52.

39. H. Choi, K. Zhang, D. D. Dionysiou, D. B. Oerther, and G. A. Sorial, "Influence of Cross-Flow Velocity on Membrane Performance During Filtration of Biological Suspension," *Journal of Membrane Science* 248 (2005): 189–199.

40. K. O. Messerian, A. Zverev, J. F. Kramarczyk, and A. L. Zydney, "Pressure-Dependent Fouling Behavior During Sterile Filtration of mRNA-Containing Lipid Nanoparticles," *Biotechnology and Bioengineering* 119 (2022): 3221–3229.

41. X. Hou, T. Zaks, R. Langer, and Y. Dong, "Lipid Nanoparticles for mRNA Delivery," *Nature Reviews Materials* 6 (2021): 1078–1094.

Supporting Information

Additional supporting information can be found online in the Supporting Information section.

18607314, 2024, 11, Downloaded from https://analyticalsciencejournals.onlinelibrary.wiley.com/doi/10.1002/bmot.202400473 by Test, Wiley Online Library on [13/11/2024]. See the Terms and Conditions (https://onlinelibrary.wiley.com/terms-and-conditions) on Wiley Online Library for rules of use; OA articles are governed by the applicable Creative Commons License